Toward Long-Lasting Large-Scale Soft Robots

The Durability Challenge in Architectured Materials

Stella, Francesco; Pei, Guanran; Meebed, Omar; Guan, Qinghua; Bing, Zhenshan; Santina, Cosimo Della; Hughes, Josie

DOI
10.1109/RoboSoft60065.2024.10521957

Publication date
2024

Document Version
Final published version

Published in
Proceedings of the IEEE 7th International Conference on Soft Robotics, RoboSoft 2024

2024 7th International Conference on Soft Robotics (RoboSoft)
San Diego, CA, USA. April 14-17, 2024

Toward long-lasting large-scale soft robots: the durability challenge in architectured materials

Francesco Stella[1,2*], Guanran Pei[1,3*], Omar Meebed[1*],
Qinghua Guan[1], Zhenshan Bing[3], Cosimo Della Santina[2,4], Josie Hughes[1]

***Abstract*— Soft robots promise groundbreaking advancements across various industries. However, soft robots are susceptible to wear, fatigue, and material degradation. Their durability and long-term reliability are often overlooked, despite being critical for the successful deployment of these systems in real-world applications. This article contributes to solving this challenge by identifying metrics that reflect material wear, mechanical hysteresis, and drift occurring during long-term operations in soft architectured materials. While this same pipeline can be generalized to different soft robots, we test these metrics on the trimmed helicoid architectured materials, and we validate the improvement in performance on the Helix soft manipulator. Thanks to the proposed metrics, we demonstrate a 75% reduction in repeatability errors over long-duration experiments.**

I. Introduction

Soft robots [1], [2] promise to revolutionize applications as diverse as minimally invasive surgery [3], search and rescue operations [4], and environmental monitoring [5]. Durability and reliability are, however, crucial for the real-world deployment of soft robots in these application domains [6]. Failure due to wear or material issues can impact both safety and task performance. Remarkably, structural softness makes these robots prone to wear and material degradation [7]. Moreover, having systems that change their dynamic as a function of prior operations makes the problem of controlling soft robots even more challenging. Despite being largely overlooked, the crucial challenge of designing soft robots with repeatable and stable behavior has attracted some attention. Prior work focused mostly on bettering materials to increase durability and robustness [8], [9], and in designing controllers able to iteratively learn the dynamics of the soft robots [10]. However, improvements in materials and control schemes alone can not provide a solution for repeatable soft robots. The geometry, fabrication method, and control modalities all affect the long-term performance [11]. Furthermore, although there is a shift towards developing benchmarks for soft robotics [12], [13], these often are task-focused and consider performance for a period of minutes rather than long-term ones.

In this work, we contribute to this challenge by identifying metrics that reflect material wear, mechanical hysteresis, and nonlinear deformations, all of which can impact performance over time. We focus the metrics and experimental study on soft robots made of architectured materials [14]. These structures are typically produced via additive manufacturing methods and offer the possibility to design soft robots at scale while having low-level control of the mechanical dynamics. The proposed metrics and experiments are ideated to be agnostic of the geometry of the architectured structure, and aimed at capturing the final performance of the soft robot, thus including the effects of material properties, stresses arising during long operations and control. Finally, we leverage these metrics to propose technical solutions for enhancing the robustness and longevity of soft robots, from a comparison of materials and manufacturing techniques to control techniques aimed at minimizing the difference in behavior over long spans of time. To summarize, this paper contributes to the state of the art in the design and characterization of soft robots with:

- metrics for the characterization of the errors arising in the long-term use of soft robots made of architectured materials,
- an analysis of the repeatability perfomance in a soft robot arm and a break down and connection of mechanical properties to its precision performance,
- comparison and characterization of several common materials and manufacturing methods for architectured materials,
- the experimental validation of the effectiveness of the metrics on a fully-fledged soft continuum arm.

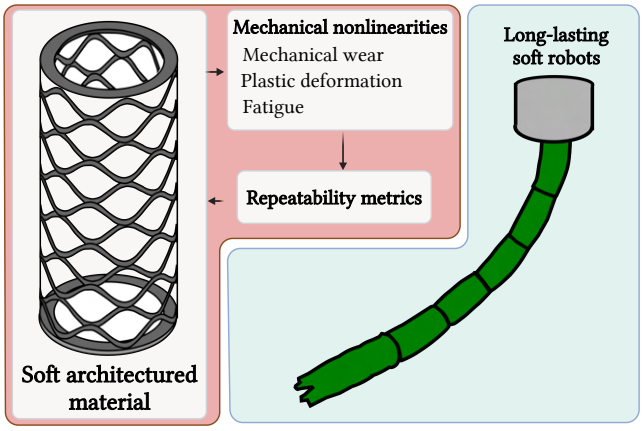

Fig. 1. A pictorial representation of the topic of this paper. Quantifying wear, plastic deformation, and fatigue can inform the design of soft continuum robots able to operate with high repeatability over long-lasting operations. We focus here on robots made of architectured materials.

*These authors contributed equally to this work. [1]CREATE Lab, EPFL, Lausanne, Switzerland. [2]Department of Cognitive Robotics, Delft University of Technology, Delft, The Netherlands. [3]Technical University of Munich, Munich, Germany. [4]Institute of Robotics and Mechatronics, German Aerospace Center (DLR), Wessling, Germany. This project was partially supported by the EU's research and innovation program EMERGE. Contact email: francesco.stella@epfl.ch.

2024 IEEE 7th International Conference on Soft Robotics (RoboSoft) | 979-8-3503-8181-8/24/$31.00 ©2024 IEEE | DOI: 10.1109/ROBOSOFT60065.2024.10521957

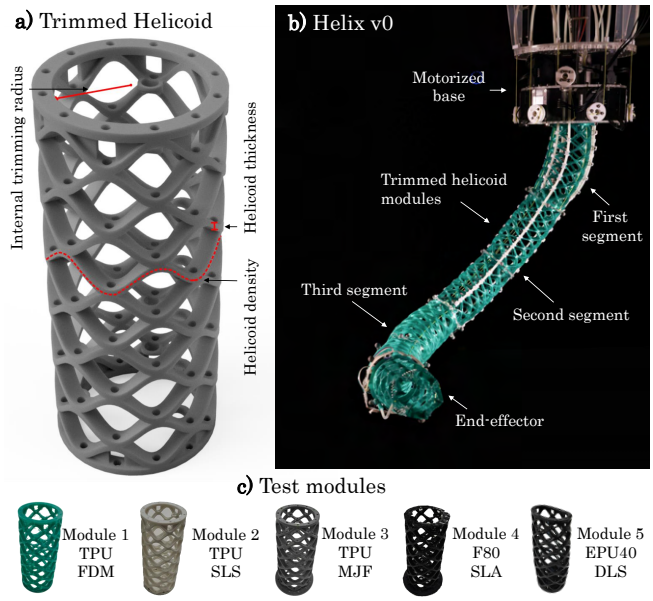

Fig. 2. **a)** The trimmed helicoid structure with its geometrical parameters highlighted. **b)** the Helix v.0 soft manipulator, composed of 5 TH modules serially connected [16]. **c)** the 5 test modules of the TH structure produced in different materials and manufacturing methods.

In the remainder of this paper, we first introduce architectured materials, after which we present the relevant metrics to evaluate the durability of soft robots. In Section III, we present the soft robot platform we use to experimentally validate the approach and characterization of the effects during extended operations. To improve the repeatability performance of the Helix Version 0 (v0) robot, 5 different trimmed helicoid modules are characterized in Section IV-C before demonstrating the improved performance of the improved Helix robot version (v1) in Section IV-E.

II. Methods

A. Architectured materials

Architectured materials are a distinct class of engineered materials characterized by precisely designed structural architectures. Unlike traditional homogeneous materials, they feature intricate, purpose-built arrangements of components at multiple length scales, offering unique and tailored mechanical properties [15]. Architectured materials have recently been applied to generate soft robots with a wide workspace, precise open-loop tracking and compliant interaction with the environment [16]. In particular, in this article, we focus on the Trimmed Helicoid (TH) architectured material, shown in Figure 2-a. The TH structure displays the ability to tune the bending to axial stiffness ratio and magnitude by varying a few geometrical parameters. In particular, the TH geometry is fully defined by its length, external radius, the inner trimmed area, the number of helicoids, and their thickness, as shown in Figure 2-a.

B. Metrics

Potential sources of loss of precision in the control of soft robots are the hysteresis of material, plastic deformations, and changes in dynamics due to mechanical fractures. Here we propose experimental metrics aimed at characterizing and evaluating their impact. In particular, we propose to use compression tests to evaluate the stiffness and dissipation of the structure, long-term repetitive motions to evaluate the stability of the structure, and a step response to characterize the steady state error and transient arising from extreme bendings. Given that soft robots composed of architectured materials are composed of modules, it is possible to perform most of the characterizations and analysis of the mechanical properties on a single unit.

1) Compression test: To evaluate the stiffness of the architectured structure and to characterize the dissipation, we perform a compression test on the modules. By comparing the area within the hysteresis curve and the area below the force-displacement curve, we can generate a material and geometry agnostic metric m_1, which evaluates the ratio between the energy inserted in the system E_{Input} and the energy dissipated by hysteresis $E_{\text{Hysteresis}}$.

2) Step response experiment: A second experiment, described in Section III-C, is designed to look at the dynamical transient and at the steady state error resulting from an extreme deformation. In the experiment, the structure is brought into a deformed state, and then suddenly released. IMUs are used to capture the evolution of the module's state. From this experiment, the modules can be compared under two metrics. The first metric, m_2, looks at the transient through the time needed to reach 80% the undeformed state. The steady-state error can be evaluated by looking at the ratio between the maximum deformation and the deformation at $t = 5m_2$.

3) Long-term drift assesment: A third experiment is designed to evaluate the drift arising in long-term repetitive motions. To this end, a motion that is relevant to the functioning of the full manipulator is repeated continuously for 1.5 hours, while monitoring with IMUs the average state per cycle. The effect of the drift is captured by the metric m_4, computed as the difference between the mean state in the first and final cycle, labeled as q_0 and q_{end} respectively, normalized by the mean state in the first cycle.

$$m_1 = \frac{E_{\text{Hysteresis}}}{E_{\text{Input}}}, \quad m_2 = \Delta t_{\Delta \text{x}=20\%\Delta \text{x}_{\max}}$$
$$m_3 = \frac{\Delta q_{\text{t}=5\text{m}_2}}{\Delta q_{\max}} \; m_4 = \frac{q_0 - q_{\text{end}}}{q_0}$$

4) Full manipulator characterization: Once the best mechanical properties for the single module are selected, it is possible to manufacture the whole soft robot, and then evaluate it on fewer metrics. In particular, we evaluate the soft robot in repeatability and dependence of the soft robot's state on its previous motion. To this end, two experiments are performed. In the first, aimed at evaluating the dependence on previous strains, the soft robot is brought to 5 different variations with increasing levels of strain, and then commanded to perform a cyclic periodic motion for 50 min. The second, designed to evaluate the effect of long-lasting strains on the soft robot's precision, the soft robot is posed in a pose with a high level of strain for varying amounts of time, and

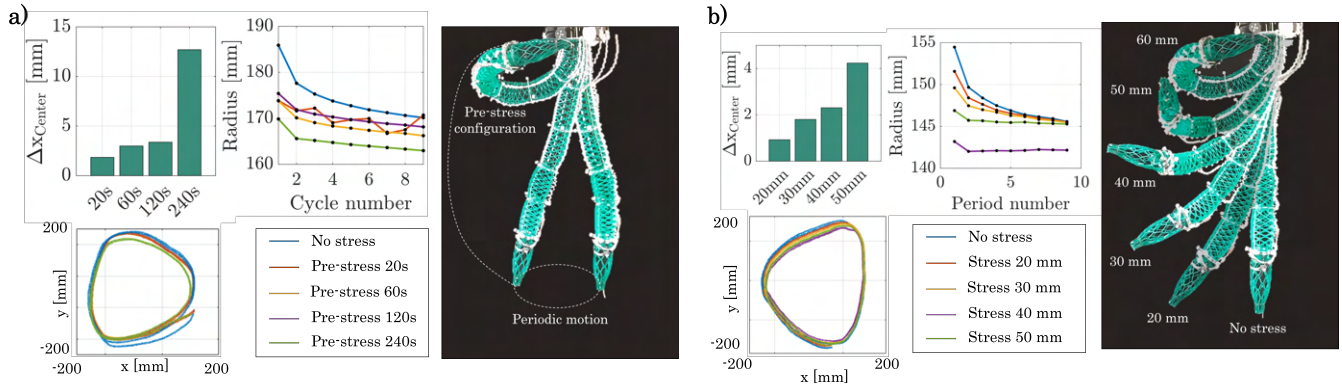

Fig. 3. **a)** During the experiment the manipulator is brought to the pre-strained configuration for varying amounts of time. The robot is then commanded to perform a periodic motion, of which we report the trajectory and errors on the centre and amplitude. **b)** During the experiment, the manipulator is pre-stressed in one of the 5 levels shown on the right. The robot is then commanded to perform a periodic motion, of which we report the trajectory, and errors on the center and amplitude.

then commanded to perform the cyclic motions for 50 mins. By looking at errors in the periodic motion it is possible to detect the dependence of the full structure on previous trajectories.

C. Manufacturing & Materials

Several versions of the TH were produced with different manufacturing methods and materials, as shown in Figure 2-c. The materials, namely Thermoplastic polyurethane (TPU), Elastomeric Polyurethane (EPU) 40 and Resione F80, were chosen to have a shore hardness in the range [50,90]A, making them suitable for soft architectured materials for large-scale soft robots. The manufacturing methods used to build the modules use state-of-the-art technologies in additive manufacturing of soft materials, such as Fused deposition modeling (FDM), Selective Laser Sintering (SLS), Multi Jet Fusion (MJF), Stereolithography (SLA) and Digital Light Synthesis (DLS). Table I provides an overview of the manufacturing technology, the 3D printer, the material shore hardness, the cost, and the manufacturing time needed to produce each unit.

III. Experimental Setups

A. Compression experiment

To characterize the stiffness and the energy loss of the different TH parts, the modules were tested in a cyclic compression test on a Zwick-Roell Z010 tensile machine. Each module was compressed to 70% their uncompressed length for six cycles. The analysis was performed in terms of strain, computed as $\frac{\Delta L}{L_0}$. The first three cycles were used to pre-condition the TH module, while the latter three were used for the characterization.

B. Shape reconstruction of the single segment

To better observe the changes in the shape and pose of soft segments, we developed an IMU module to record the absolute orientation of the tip of the soft segment, enabling us to reconstruct the shape and pose of the soft segment. Thanks to the powerful computational capabilities of the Teensy 4.0 MCU and the high update frequency of the Adafruit LSM6DSOX + LIS3MDL sensors, when integrating the data with a Madgwick filter [17], the IMU module can theoretically achieve a 500Hz update rate. Therefore, the IMU module can rapidly and accurately capture the absolute orientation data at the top of the soft segment. Before the step response experiment, the soft segments are placed straight for calibration. Then, during the experiment, the IMU module is used to record the absolute orientations at the top of the calibrated soft segments as the reference values. After obtaining the relative orientation at the top of the soft segment, we applied the soft segment reconstruction method based on the PCC model as proposed in [18].

$$\Delta_x = \frac{1}{2}(R(3,1) - R(1,3))\frac{\arccos(R(3,3))}{\sin(\arccos(R(3,3)))} \quad (1)$$

$$\Delta_y = \frac{1}{2}(R(3,2) - R(2,3))\frac{\arccos(R(3,3))}{\sin(\arccos(R(3,3)))} \quad (2)$$

$$\Delta = \sqrt{\Delta_{\mathrm{x}}^2 + \Delta_{\mathrm{y}}^2} \quad (3)$$

where R represents the relative orientation of the soft segment's tip. Δ_x and Δ_y are the innovative improved state parameters for soft robots presented in [19]. When employing the novel parametrization, the system can tackle more intricate tasks, significantly lowering the computational load, all while avoiding spikes and discontinuous behaviors. These two variables encompass comprehensive data pertaining to the classic parametrization ϕ and θ, while simultaneously maintaining a direct correlation with physical parameters. In order to facilitate a more intuitive observation of the changes in the soft segment's shape, we employ the formula proposed in [19] to convert the state parameters of soft segments from Δ_x and Δ_y into ϕ and θ.

$$\phi\,(q) = \arccos\left(\frac{\Delta_{\mathrm{x}}}{\Delta}\right) = \arcsin\left(\frac{\Delta_{\mathrm{y}}}{\Delta}\right) \quad (4)$$

$$\theta\,(q) = \frac{\Delta}{d} \quad (5)$$

TABLE I

COMPARISON OF THE DIFFERENT MODULES IN TERMS OF PRINTING TECHNOLOGY, MATERIAL, COST AND MANUFACTURING TIME.

Tech	Printer	Material	Shore hardness	Cost ($)	Manufacturing time
FDM	Flashforge Creator Pro 2	TPU	53D	~ 5	9h
SLS	–	TPU	90A	~ 28	-
MJF	HP Jet Fusion 5200	TPU01	88A	~ 80	-
SLA	Creality Halot-mage pro	Resione F80	50-60A	~ 5	8h
DLS	Carbon M1	Carbon EPU40	68A	~ 40	12h

where ϕ represents the angle in the z-axis between the cross-section where the soft segment bends and the reference cross-section without the soft segment's bending, and θ represents the central angle, measured in degrees, corresponding to the arc length of the soft segment under the assumption of the PCC model. In addition, d represents the distance from the geometric center of the cross-section to the tendons that are symmetrically distributed on the cross-section of the soft segment. Using the aforementioned method, we can reconstruct the shape and pose of soft segments from the data collected by the IMU module. This forms the foundation for evaluating the experimental performance of different soft segments, i.e. in the step response experiment and cyclic long-term experiment, we evaluate the stability and durability of different kinds of soft segments by observing the variation of their curvature θ.

C. Step response setup

In order to measure the rate and stability of the shape recovery in soft segments after extreme deformations, each module was pre-deformed by a UR-5 manipulator as shown in Figure 6. Between experiments, the same orientation ϕ and curvature θ were kept for every module. The modules were then released in a controlled way by moving the UR5 away from the module. By employing the IMU-based soft segment shape and pose reconstruction method the shape and pose of soft segments are recorded.

D. Cyclic long-term setup

To capture the stability over longterm motions, a simple platform based on 3 motors was designed. The module is then connected to the motors through cables running along its body. The module was controlled in open-loop into a periodic circular motion, computed as inverse kinematics of continuum robots [20]. For each segment the circular motion was repeated continuously for 1.5 hours, and the IMU module was used to measure the absolute orientation of the tip of each soft segment. The setup of this experiment is shown in Figure 5. Thanks to this setup, we recorded the drift occurring in each soft segment durating long repetitive motions.

E. Full manipulator experiments

The Helix robot [16] was used as an experimental setup to test a fully-fledged soft manipulator composed of five TH modules. Each segment of the arm is actuated by tendons and motors (Dynamixel XM430-W210-R). Three of these actuators control the pose of the first segment, where the pose is defined as the segment compression, flexion and orientation around the vertical axis. Similarly, three other actuators control the pose of the second and third modules simultaneously while the final three control the pose of the fourth and fifth modules. The manipulation is placed within a motion capture environment (Optitrack), which is used to capture the pose of the manipulator.

IV. RESULTS

A. Characterization of the performances of Helix v.0

To benchmark the loss of repeatability arising in architectured material-based soft manipulators, the experiments described in Section II-B were performed on the Helix v.0 robot, composed of FDM-TPU modules.

To test the long-term performance of the green arm, the robot is first brought for a selected time frame in a deformed state, which is then followed by a periodic motion, used to evaluate its repeatability. The periodic motion is used to evaluate the variation of this periodic trajectory as a function of manipulator deformation induced from previous trajectories. In Figure 3-a, the effect of the time spent in a deformed state on the repeatability of the arm is reported. It is possible to notice that increasing the duration of pre-bending leads to a higher shift in the subsequent trajectories and that this effect is then tamed during the next repetitions, in which the manipulator reaches a stable behavior. Similarly, in Figure 3-b, it is possible to observe that an increase in pre-stress of the arm leads to higher shifts in the subsequent trajectories and that this effect is gradually reduced with the repetitions of the periodic cycles. The highest shift in trajectory observed was captured for a long duration of high pre-stress and was 13 mm, i.e. 1.5$\%$ the manipulator's length. The following analysis performed on single modules is therefore aimed at selecting a version that leads to a manipulator with a higher grade of repeatability.

B. Compression test

The force-strain curves of the 5 different modules are reported in Figure 4. Table II shows the axial stiffness and the energy dissipation metric m_1 for each module. These values are crucial to developing quasi-static [21] and dynamical models of soft manipulators [22], [23]. In particular, the axial stiffness of the modules EPU40-DLS and F80-SLA was too low to sustain the weight of the assembled soft manipulator.

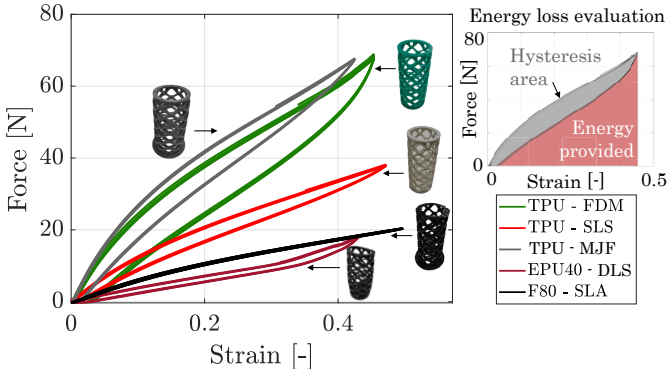

Fig. 4. On the left, the force-strain curves for the 5 modules. On the top right, a representation of the hysteresis area against the energy provided.

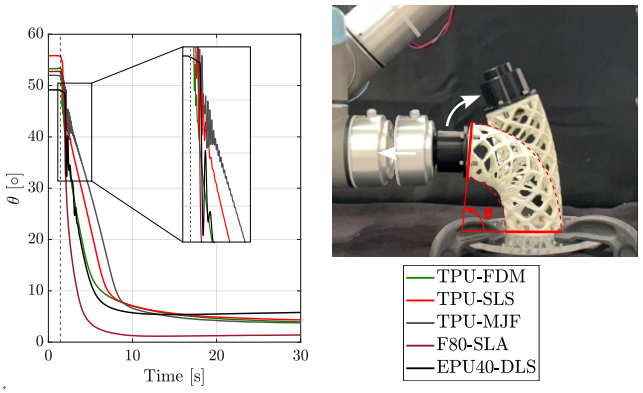

Fig. 6. Step response of the 5 modules. A UR5, shown in the top-right, pre-bends the structure to 50% and releases it in a controlled way.

C. Step response performance

To assess and compare the stability and deformation recovery capability of soft segments made from 5 different methods or materials, we measured the step response of each kind of soft segment. In the experiment, all the soft segments are bent to θ_{init} is $52.5°$, and then unconstrain UR5 so that the soft segments are free to recover their shapes. The step response experiment was repeated five times for each soft segment, and the average of the five measurements was taken as the average of the curvature trajectory measurements for each kind of soft segment. Thanks to this experiment, we evaluated the metrics m_2 and m_3, reported in Table II, to evaluate the early stage deformation recovery rate and the steady deformation recovery after 5 times m_2 time.

In Figure 6 we report the evolution of the bendingθ for five different types of soft segments over time in the step response experiment. The F80-SLA soft segment not only exhibits the fastest initial deformation recovery rate but also boasts the highest steady deformation recovery amount. Correspondingly, it has the lowest values for both m_2 and m_3, as shown in Table II. Among the other four soft segments, EPU40-DLS demonstrates the highest rate of deformation recovery, followed by TPU-FDM, TPU-SLS in the next position, and TPU-MJF exhibiting the lowest rate of deformation recovery. Exactly the same as indicated by

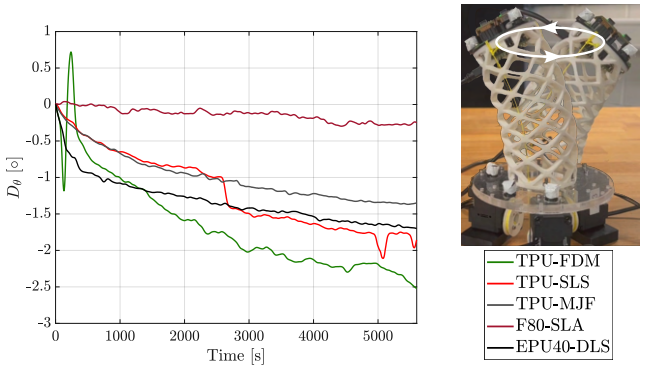

Fig. 5. Curvature trajectories of long-term periodic movements for 5 kinds of soft segments. Over the 1.5 hours of experiment it is possible to notice a clear drift, in the order of [0.1-1.5]° depending on the module properties.

TABLE II
METRIC COMPARISON FOR EACH ELEMENT

Module	1	2	3	4	5
Tech	FDM	SLS	MJF	SLA	DLS
Material	TPU	TPU	TPU	F80	EPU40
$\mathbf{k_{axial}}$ [N/mm]	1.07	1.13	0.57	0.28	0.29
$\mathbf{m_1}$	0.18	0.12	0.14	0.03	0.10
$\mathbf{m_2}$	6.3	6.6	7.8	3.41	5.55
$\mathbf{m_3}$	0.08	0.06	0.075	0.02	0.1
$\mathbf{m_4}$	0.15	0.08	0.07	0.02	0.08

the m_2 metric in Table II. In addition, the soft segment of EPU40-SLA exhibits the poorest performance in terms of steady deformation recovery. Furthermore, the soft segments of TPU-FDM, TPU-SLS and TPA-SLS have the almost same steady deformation recovery mount. In the step response experiment, besides observing the deformation recovery of the soft segments, another noteworthy parameter is the self-oscillation generated by the soft segments during the deformation recovery process. Self-oscillation significantly impacts the rate of deformation recovery of the soft segments, with stronger self-oscillation leading to a slower state recovery rate. As depicted in the zoomed-in section in Figure 6, TPU-MJF exhibits the highest self-oscillation frequency and the second-largest amplitude, which consequently results in the slowest deformation recovery rate.

D. Cyclic long-term performance

During the cyclic longterm test, we control each soft segment to keep its shape curvature κ constant at 10 and trunk length s constant at 0.12 meters during the movement, and constantly change its orientation (from 0 to 2π) so that its tip can complete the periodic circular movements. The averaged absolute drift D_θ of the shape parameter θ for every kind of soft segment is presented in Figure 5. This is calculated as $D_\theta = \theta_{end} - \theta_0$ where θ_0 represents the soft segment's state parameter θ at the beginning of the experiment. Furthermore, θ_{end} signifies the soft segment's state parameter θ at the end of the experiment. According to Figure 5, it is possible to observe that all the soft

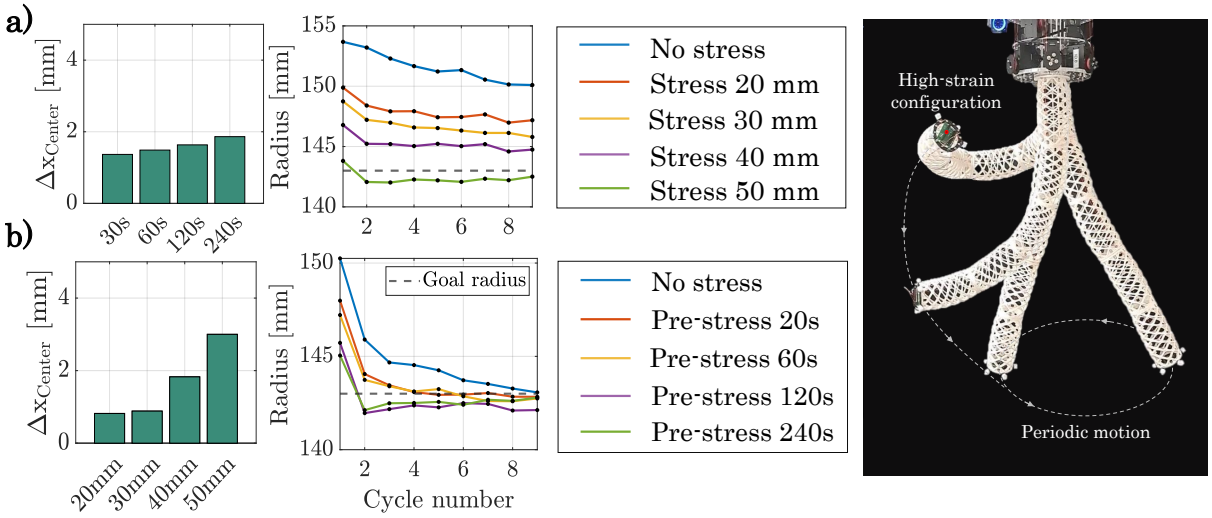

Fig. 7. On right the Helix v1.0 manipulator in the extreme poses reached during the experiments**a)** During the experiment the manipulator is brought to the pre-strained configuration for varying amounts of time. The robot is then commanded to perform a periodic motion, of which we report the trajectory and errors on the center and amplitude. **b)** During the experiment, the manipulator is pre-stressed in one of the 5 levels shown on the right. The robot is then commanded to perform a periodic motion, of which we report the trajectory, and errors on the center and amplitude.

segments are affected by the issue of drift, and as the cyclic circular movements continue, the drift in the state parameter θ steadily increases.

By counting the absolute drifts of these five types of soft segments, we can see that the soft segment of F80-SLA always maintains the smallest absolute motion drift during the experiment and the soft segment of the TPU-FDM produces the largest absolute at the end of the experiment. In addition, the soft segment of TPU-SLS and TPU-MJF have almost the same performance in the first half of the test, but afterward, the soft segment of TPU-SLS generates a larger motion drift. The soft segment of EPU40-DLS displays the maximum rate of drift at the beginning stage of the experiment. However, the total motion drift after 1.5 hours of experiment is smaller than TPU-FDM. The observed trends in Figure 5 correspond precisely to the m_4 metric in Table II-B. Specifically, TPU-FDM exhibits the highest m_4 value, indicating the maximum relative motion drift, while F80-SLA shows the lowest relative motion drift.

E. An improved soft continuum arm

Based on the metrics in Table II, the TPU-SLS module was selected. Within this batch, this module displays the best trade-off between goal stiffness, cost, damping factor, long-term drift and steady-state error after deformation. The F80-SLA module, showing the least hysteresis and the lowest steady-state error was not selected for its low stiffness. Therefore a new manipulator, the Helix v.1, shown in Figure 7, was manufactured with TPU-SLS modules following the design of the Helix v.0 structure. To compare the new version with the soft robot composed of TPU-FDM modules, the Helix 1.0 version was tested with the experiments defined in Section III-E. As a result of the study, the improved version exhibits higher performances in terms of repeatability and long-term drift. The results of the experiments in Figure 7, show that the Helix v1.0 demonstrates higher accuracy with respect to the Helix v.0 for both long-duration strains and for high pre-stresses. In particular, when comparing the extreme cases, the shift in trajectory is reduced to 25% the error shown by the previous version of the manipulator. Moreover, the transition to a repeatable motion is achieved within the first 2 cycles of periodic motions, which is significantly faster than the recovery shown by the previous manipulator, as shown in Figure 7-b.

Thanks to the advantages of the SLS manufacturing process, Helix v1.0 demonstrates improved elasticity and resistance to plastic deformation compared to Helix v.0. Therefore, in our time-based pre-stress periodic motion experiment, for pre-stress durations of 20s, 60s, and 120s, Helix v1.0 exhibits an average ΔX_{Center} that is 50% smaller than that of Helix v.0. In the case of a pre-stress duration of 240s, Helix v1.0's performance is even more remarkable, with ΔX_{Center} decreasing to approximately one-sixth of Helix v.0's ΔX_{Center}. Additionally, in the length-based pre-stress periodic motion experiment, except for the 20mm pre-stress scenario, Helix v1.0's average ΔX_{Center} is 25% smaller than that of Helix v.0. Moreover, according to the line chart depicting the variation of radius with cycle number in Figure 3 and 7. We can clearly observe that in both the time-based pre-stress experiment and the length-based pre-stress experiment, the radius trend line for Helix v1.0 is smoother. Furthermore, for different pre-stress configurations, the steady-state values for Helix v1.0 are more similar, indcating negligible effects of previous stresses on the motion. This is particularly notable in the extreme stress cases of pre-stress 240s and pre-stress 50mm, both exhibiting a behavior close to the 'no stress' scenario.

V. Discussion and Conclusion

In this article, we approach the pressing challenge of durability and long-term reliability of soft robots. Focusing on architectured materials, particularly the Trimmed Helicoid structure, we compare different state-of-the-art materials and additive manufacturing techniques, providing insights into the mechanical properties, cost, and manufacturing time of architectured structures for soft robots. We then introduce metrics for assessing the durability and stability of soft robots, offering a systematic way to evaluate the long-term performance of soft robots, including their response to repetitive motions and dependence on previous strain. We conclude by demonstrating the effectiveness of these metrics by comparing the performance of a fully-fledged manipulator composed of the architectured material selected through the metrics and a baseline manipulator designed without this analysis.

In conclusion, the article highlights the importance of considering durability and long-term reliability as fundamental aspects in the development of soft robots. By addressing these challenges, researchers and engineers can make soft robots more robust and dependable, opening up new possibilities for their application in critical domains.

References

[1] F. Stella and J. Hughes, "The science of soft robot design: A review of motivations, methods and enabling technologies," *Frontiers in Robotics and AI*, vol. 9, p. 1059026, 2023.

[2] C. Della Santina, M. G. Catalano, A. Bicchi, M. Ang, O. Khatib, and B. Siciliano, "Soft robots," *Encyclopedia of Robotics*, vol. 489, 2020.

[3] J. Rosen, L. N. Sekhar, D. Glozman, M. Miyasaka, J. Dosher, B. Dellon, K. S. Moe, A. Kim, L. J. Kim, T. Lendvay *et al.*, "Roboscope: A flexible and bendable surgical robot for single portal minimally invasive surgery," in *2017 IEEE International Conference on Robotics and Automation (ICRA)*. IEEE, 2017, pp. 2364–2370.

[4] E. W. Hawkes, L. H. Blumenschein, J. D. Greer, and A. M. Okamura, "A soft robot that navigates its environment through growth," *Science Robotics*, vol. 2, no. 8, p. eaan3028, 2017.

[5] P. A. Der Maur, B. Djambazi, Y. Haberthür, P. Hörmann, A. Kübler, M. Lustenberger, S. Sigrist, O. Vigen, J. Förster, F. Achermann *et al.*, "Roboa: Construction and evaluation of a steerable vine robot for search and rescue applications," in *2021 IEEE 4th International Conference on Soft Robotics (RoboSoft)*. IEEE, 2021, pp. 15–20.

[6] G. Giordano, S. P. Murali Babu, and B. Mazzolai, "Soft robotics towards sustainable development goals and climate actions," *Frontiers in Robotics and AI*, vol. 10, p. 1116005, 2023.

[7] F. Hartmann, M. Baumgartner, and M. Kaltenbrunner, "Becoming sustainable, the new frontier in soft robotics," *Advanced Materials*, vol. 33, no. 19, p. 2004413, 2021.

[8] J. Amend, N. Cheng, S. Fakhouri, and B. Culley, "Soft robotics commercialization: Jamming grippers from research to product," *Soft robotics*, vol. 3, no. 4, pp. 213–222, 2016.

[9] Y. Wang, C. Gregory, and M. A. Minor, "Improving mechanical properties of molded silicone rubber for soft robotics through fabric compositing," *Soft robotics*, vol. 5, no. 3, pp. 272–290, 2018.

[10] M. Pierallini, F. Stella, F. Angelini, B. Deutschmann, J. Hughes, A. Bicchi, M. Garabini, and C. Della Santina, "A provably stable iterative learning controller for continuum soft robots," *IEEE Robotics and Automation Letters*, 2023.

[11] Y. L. Yap, S. L. Sing, and W. Y. Yeong, "A review of 3d printing processes and materials for soft robotics," *Rapid Prototyping Journal*, vol. 26, no. 8, pp. 1345–1361, 2020.

[12] M. A. Graule, T. P. McCarthy, C. B. Teeple, J. Werfel, and R. J. Wood, "Somogym: A toolkit for developing and evaluating controllers and reinforcement learning algorithms for soft robots," *IEEE Robotics and Automation Letters*, vol. 7, no. 2, pp. 4071–4078, 2022.

[13] T. Watanabe, K. Yamazaki, and Y. Yokokohji, "Survey of robotic manipulation studies intending practical applications in real environments-object recognition, soft robot hand, and challenge program and benchmarking," *Advanced Robotics*, vol. 31, no. 19-20, pp. 1114–1132, 2017.

[14] F. Barthelat, "Architectured materials in engineering and biology: fabrication, structure, mechanics and performance," *International Materials Reviews*, vol. 60, no. 8, pp. 413–430, 2015.

[15] M. Ashby, "Designing architectured materials," *Scripta Materialia*, vol. 68, no. 1, pp. 4–7, 2013.

[16] Q. Guan, F. Stella, C. Della Santina, J. Leng, and J. Hughes, "Trimmed helicoids: an architectured soft structure yielding soft robots with high precision, large workspace, and compliant interactions," *npj Robotics*, vol. 1, no. 1, p. 4, 2023.

[17] S. Madgwick *et al.*, "An efficient orientation filter for inertial and inertial/magnetic sensor arrays," *Report x-io and University of Bristol (UK)*, vol. 25, pp. 113–118, 2010.

[18] J. Hughes, F. Stella, C. D. Santina, and D. Rus, "Sensing soft robot shape using imus: An experimental investigation," in *Experimental Robotics: The 17th International Symposium*. Springer, 2021, pp. 543–552.

[19] C. Della Santina, A. Bicchi, and D. Rus, "On an improved state parametrization for soft robots with piecewise constant curvature and its use in model based control," *IEEE Robotics and Automation Letters*, vol. 5, no. 2, pp. 1001–1008, 2020.

[20] B. A. Jones and I. D. Walker, "Kinematics for multisection continuum robots," *IEEE Transactions on Robotics*, vol. 22, no. 1, pp. 43–55, 2006.

[21] F. Stella, J. Hughes, D. Rus, and C. Della Santina, "Prescribing cartesian stiffness of soft robots by co-optimization of shape and segment-level stiffness," *Soft Robotics*, 2023.

[22] F. Stella, Q. Guan, C. Della Santina, and J. Hughes, "Piecewise affine curvature model: a reduced-order model for soft robot-environment interaction beyond pcc," in *2023 IEEE International Conference on Soft Robotics (RoboSoft)*. IEEE, 2023, pp. 1–7.

[23] F. Stella, N. Obayashi, C. Della Santina, and J. Hughes, "An experimental validation of the polynomial curvature model: identification and optimal control of a soft underwater tentacle," *IEEE Robotics and Automation Letters*, vol. 7, no. 4, pp. 11 410–11 417, 2022.